



CHORUS

This is the accepted manuscript made available via CHORUS. The article has been published as:

Impact of chaos and Brownian diffusion on irreversibility in Stokes flows

P. Sundararajan, J. D. Kirtland, D. L. Koch, and A. D. Stroock

Phys. Rev. E **86**, 046203 — Published 4 October 2012

DOI: [10.1103/PhysRevE.86.046203](https://doi.org/10.1103/PhysRevE.86.046203)

1 Impact of chaos and Brownian diffusion on irreversibility in Stokes flows

2 Sundararajan, P.¹, Kirtland, J.D.², Koch, D.L.³, Stroock, A.D.^{3,4*}

3 ¹Sibley School of Mechanical and Aerospace Engineering, Cornell University, Ithaca, NY
4 14853, USA, ²Department of Physics and Astronomy, Alfred University, One Saxon Drive,
5 Alfred, NY, 14802, USA, ³Department of Chemical and Biomolecular Engineering, Cornell
6 University, Ithaca, NY, 14853, USA, ⁴Kavli Institute at Cornell for Nanoscale Science, Cornell
7 University, Ithaca, NY, 14853, USA

8 (Received September 19, 2012)

9 We study a reversal process in Stokes flows in the presence of weak diffusion in order to clarify
10 the distinct effects that chaotic flows have on the loss of reversibility relative to non-chaotic
11 flows. In all linear flows, including a representation of the baker's map, we show that the decay
12 of reversibility presents universal properties. In nonlinear chaotic and non-chaotic flows, we
13 show that this universality breaks down due to the distribution of strain rates. In the limit of
14 infinitesimal diffusivity, we predict qualitatively distinct behavior in the chaotic case.

15 PACS numbers: 05.70.Ln, 05.45.Ac, 47.15.G-, 87.80.Qk

16
17 **I. INTRODUCTION**

18 A debate persists on whether dynamical chaos is the origin of irreversibility in the contexts of
19 statistical mechanics [1-2] and transport phenomena [3-4]. On the one hand, running forward in
20 time, chaotic systems, like the multibaker mapping exhibit loss of time correlation and diffusive-
21 like dynamics [5]. On the other hand, chaos is not intrinsically irreversible, in that, with infinite
22 precision and in the absence of sources of random noise, chaotic trajectories will return to their
23 original locations in phase space if the dynamics is reversed [6]. Experimental studies indicate
24 that non-Brownian particles in oscillatory shear exhibit irreversibility and chaotic dynamics [3-
25 4], but the relative importance of chaos and solid body contacts in preventing reversibility of the
26 trajectories of the particles is not clear [7]. A challenge in defining the impact of chaos on
27 irreversibility arises from the well-appreciated fact that chaotic flows accelerate the loss of

28 reversibility in the presence of noise or finite precision relative to non-chaotic flows. In this
29 Letter, we adapt an analytical treatment of mixing (simultaneous convection and diffusion) put
30 forth by Ranz [8] to scale the dynamics of diffusive tracers in a reversal experiment with respect
31 to the characteristic rate of mixing. This approach elucidates a unity in the evolution of
32 convective diffusive irreversibility in all linear flows and shows how this unity is disrupted by
33 the presence of the distribution of strain rates in both chaotic and non-chaotic flows.

34 The reversal experiment that we consider is based on Heller’s proposal [9-10] to use diffusive
35 irreversibility in time-reversible Stokes flows as a means to separate solutes of distinct Brownian
36 diffusivity from a mixture. Figure 1 illustrates his proposal for a mixture of two solutes: i) stir the
37 mixture [yellow region in Fig. 1(a)] until the distribution of the solute with higher diffusivity
38 (green) has been largely homogenized into a carrier fluid [black region in Fig. 1(a)], ii) “unstir”
39 (reverse the flow) to completely undo the deformation [Fig. 1(c)], and iii) collect the fluid from
40 the original volume. The collected fluid will be partially purified of the tracers of higher
41 diffusivity. We call this process separation by convective diffusive irreversibility, SCDI. In
42 considering SCDI, Aref and Jones [11] defined return fraction R_f – the fraction of diffusive
43 tracers that return to the original volume [Fig. 1(c)] – as a measure of reversibility. They showed
44 that R_f decays faster in chaotic flows relative to non-chaotic flows for any amplitude of
45 diffusivity and concluded that chaotic dynamics could, in this sense, enhance separation of
46 diffusive solutes. Ottino [12] and others [13] have demonstrated experimentally this acceleration
47 of the decay of reversibility by chaotic dynamics.

48 We now extend this investigation to ask further how chaotic flows impact the efficiency of SCDI
49 relative to pure diffusion and non-chaotic flows. For this purpose, we define the maximum
50 differential reversibility:

51
$$\phi(D_{high}, D_{low}) = \text{Max} \left(\frac{R_f(t_{stir}, D_{low})}{R_f(t_{stir}, D_{high})} \right)_{\forall t_{stir}} . \quad (1)$$

52 This function is the maximum ratio of return fractions of tracers of distinct diffusivities D_{high} and
 53 D_{low} with respect to stirring time. This differential reversibility measures the sensitivity of
 54 reversal to differences in diffusive noise (a higher value of ϕ indicates greater sensitivity) and
 55 can serve as a figure of merit for its efficiency for SCDI; ϕ also provides a rate independent
 56 observable with which to compare the reversal process in the presence and absence of chaos.

57 **II. RANZ MODEL**

58 We first consider SCDI in three simple cases – (i) no flow such that the tracers evolve by pure
 59 diffusion; (ii) pure extensional flow such that the fluid undergoes deformation at an exponential
 60 rate; and (iii) simple shear flow such that the fluid undergoes deformation at an algebraic rate.
 61 Pure extension and simple shear are linear flows [14]. The work of Ranz [8] indicates that, for
 62 weak diffusion, mixing of a periodic array of bands of solute in linear flows [Fig. 2(a)] can
 63 capture mixing in the more general nonlinear flows because 1) the folding by a general flow
 64 typically results in an approximate spatial periodicity (λ) in the concentration field over short
 65 distances, and 2) the flow is approximately linear over short distances. In the case of pure
 66 extension, the evolution of these periodic strands represent mixing by the baker’s transformation,
 67 a canonical model of chaotic dynamics [15]. These strands, when observed in the local frame of
 68 reference (x', y') [Fig. 2(a); in which we translate and rotate with the strand] experience an
 69 effective rate of extension along y' of $\alpha(t, \dot{\gamma}) = -d \ln[(s(t)/s(0))]/dt$ where $s(t)$ is the width of the
 70 strand at time t and $\dot{\gamma}$ is the actual strain rate in the flow. For simple shear flow, $\alpha = \dot{\gamma}/[1 + (\dot{\gamma})^2]$

71 and for extensional flow, $\alpha = \dot{\gamma}$. In this local frame (x', y') , the convection diffusion equation
 72 has the form:

$$73 \quad \frac{\partial c}{\partial t} - \alpha x' \frac{\partial c}{\partial x'} = D \frac{\partial^2 c}{\partial x'^2}. \quad (2)$$

74 We non-dimensionalize time and position using the Ranz transformation:

$$75 \quad \xi = x'/s(t) \text{ and } \tau = \int_0^t D dt'/s(t')^2. \quad (3)$$

76 The mixing time for extension τ_{ext} , simple shear τ_{ss} , and pure diffusion τ_d are

$$77 \quad \tau_{ext} = \frac{D[\exp(2\dot{\gamma}t) - 1]}{2\dot{\gamma}s_0^2}, \quad \tau_{ss} = \frac{D[\dot{\gamma}t + (\dot{\gamma}t)^3/3]}{\dot{\gamma}s_0^2}, \text{ and } \tau_d = \frac{Dt}{s_0^2}. \quad (4)$$

78 Physically, the mixing time, τ represents the time required for a distribution of solute
 79 undergoing pure diffusion to reach the same state as the distribution would in the flow under
 80 consideration after a dimensional time, t .

81 The non-dimensionalization in Eq. (3) reduces the convection-diffusion equation (2) to a
 82 transient diffusion equation:

$$83 \quad \frac{\partial c}{\partial \tau} = \frac{\partial^2 c}{\partial \xi^2}. \quad (5)$$

84 The transformation to Eq. (5) indicates that the full dynamics of convection-diffusion in linear
 85 flows can be captured by a purely diffusive process in the $\xi\tau$ -domain with a non-dimensional
 86 diffusivity of one.

87 We can treat SCDI in these flows in a simple manner: using Eq. (5), we model the stirring phase
 88 by tracking the evolution of the initial distribution, $c(\xi, \tau = 0)$ for $\tau_{stir}(\dot{\gamma}_{stir}, D)$, and the un-

89 stirring phase by tracking the evolution of the stirred distribution, $c(\xi, \tau_{stir})$ for an additional
90 $\tau_{unstir}(\dot{\gamma}_{unstir}, t_{unstir}, D)$. Using the conditions for complete un-stirring, $t_{stir} = t_{unstir}$, and $\dot{\gamma}_{unstir} = -\dot{\gamma}$
91 , we find that $\alpha(t_{unstir}, \dot{\gamma}_{unstir}) = \alpha(t_{stir}, -\dot{\gamma}) = -\alpha(t_{stir}, \dot{\gamma})$. Upon integrating Eq. (3), we find that
92 $\tau_{stir} = \tau_{unstir}$. Hence the final distribution after stirring and un-stirring is simply $c(\xi, 2\tau_{stir})$. Figure
93 2(b) shows analytical solutions of Eq. (5) during the evolution of the initial square wave
94 distribution. We evaluate $R_f(\tau_{stir})$ in the $\xi\tau$ -domain as the ratio of the integrated concentration
95 $c(\xi, 2\tau_{stir})$ [shaded area in Fig. 2(b)] within the interval $(-0.5 \leq \xi \leq 0.5)$ to the integrated initial
96 concentration $c(\xi, \tau = 0)$ within the same interval. Further, $\phi(D_{high}, D_{low})$ can be evaluated from
97 R_f with Eq. (1). Given the same initial condition and governing equation, the solutions and
98 measures of reversibility are the same for all linear flows. Thus, using the Ranz transformation
99 [Eq. (3)], we elucidate a unity in the decay of reversibility, R_f and of the maximum differential
100 reversibility, $\phi(D_{high}, D_{low})$ in all convection-diffusion processes that are governed by Eq. (5). To
101 appreciate the impact of the Ranz transformation, figures 2(c) and 2(d) show the rapid decay of
102 return fraction as a function of total strain $\dot{\gamma}t$ in an extensional flow relative to that in a simple
103 shear as observed by Aref and Jones [11]. Transforming to the τ -domain in figure 2(e) [using
104 Eq. (4)], the decay of R_f collapses into a single master return curve and this collapse results in a
105 single master curve for differential reversibility [Fig. 2(f)]. We conclude that the exponential
106 separation and the resulting sensitivity to noise in chaotic flows accelerate the decay of
107 reversibility, but do not, on their own, disrupt the universality observed with the Ranz
108 transformation or change differential reversibility relative to other linear flows.

109

110 **III. NUMERICAL SIMULATION**

111 We will now study SCDI in nonlinear velocity fields using the chaotic sine flow [16] and the
 112 non-chaotic steady Taylor-Green vortex flow [17] as examples (Fig. 3). In the chaotic case [Fig.
 113 3(b), first row], the flow switches between two orthogonal sine flows with a period, $T_{cyc} \equiv 1$ as
 114 given in Eqs. (6) and (7); in the non-chaotic case [Fig. 3(b), second row], the two sine flows
 115 operate continuously as given in Eq. (8).

116
$$u_x = 1.75 \sin(2\pi x); u_y = 0; nT_{cyc} \leq t < 0.5(2n+1)T_{cyc}; n = 0, 1, 2, \dots \quad (6)$$

117
$$u_x = 0; u_y = 1.75 \sin(2\pi y); 0.5(2n+1)T_{cyc} \leq t < (n+1)T_{cyc}; \quad (7)$$

118
$$u_x = 0.6125 \sin(\pi x) \cos(\pi y); u_y = 0.6125 \sin(\pi y) \cos(\pi x); \quad (8)$$

119 The flows evolve forward [stirring, Fig. 3(b)] for a time, t (number of cycles for chaotic case)
 120 and then backward [un-stirring, Fig. 3(d)] for the same time, t . We note that this chaotic sine
 121 flow does not contain any non-chaotic islands. We simulate the evolution of the concentration
 122 profiles of a mixture of solutes of different diffusivities [Fig. 3(a)] with Lagrangian diffusive
 123 particle tracking as shown in figure 3. Briefly, the Lagrangian diffusive particle tracking method
 124 involves the following [18]: (a) populate the domain [Fig. 3(a)] using 10^6 particles randomly; (b)
 125 track the positions of the particles \vec{x} in the chaotic and non-chaotic flows by solving for the
 126 particle trajectories $\frac{d\vec{x}}{dt} = \vec{u} + \vec{B}(t)$, where \vec{u} is the velocity [as shown in Fig. 3(b) and 3(d)], and
 127 $\vec{B}(t)$ is the stochastic contribution to the velocity that represents diffusion; (c) obtain the
 128 concentration profiles [Fig. 3(a)] by binning particle positions at chosen times.

129

130 **IV. RESULTS AND DISCUSSION**

131 **A. Comparison with the Ranz model**

132 In figures 4(a) and 4(b), we plot $R_f(\dot{\gamma}, D)$ calculated with respect to the original volume
133 bounded by the dashed white lines in figure 3(e) for each flow. Noting the similarity in
134 $R_f(\dot{\gamma}, D)$ in figures 4(a) and 4(b) (chaotic and non-chaotic flows) and figures 2(c) and 2(d)
135 (extension and simple shear), we plot R_f as a function of the mixing time, τ . For this purpose,
136 we use $\tau_{\langle\dot{\gamma}\rangle}$ defined for linear flows in Eq. 4 (τ_{ext} for chaotic and τ_{ss} for non-chaotic flows, with
137 two parameters, the mean strain rate, $\langle\dot{\gamma}\rangle$ that we calculate independently and the initial strand
138 thickness, s_0 as an adjustable fitting parameter). Figure 4(c) shows that $R_f(\tau_{\langle\dot{\gamma}\rangle})$ appears to
139 collapse for each class of flow for a range of diffusivities ($D = 5.7 \times 10^{-7} - 5.7 \times 10^{-10}$), but not
140 onto the master return curve for linear flows [black line replotted from Fig. 2(e)]. We also find
141 that the evolution of $\phi(D_{high}, D_{low})$ in chaotic flows and that in non-chaotic flows are distinct
142 from each other and from that in linear flows [Fig. 4(d)]. The universal behavior of R_f and ϕ
143 observed for linear flows does not generalize to nonlinear flows. Interestingly, the maximum
144 differential reversibility is the smallest for the chaotic case. This observation indicates that, while
145 chaos accelerates the absolute rate of decay of reversibility due to diffusion, it reduces the
146 sensitivity to differences in diffusivity for nonlinear flows.

147 **B. Modified Ranz model**

148 We search for the origin of the distinct evolution of reversibility in linear and nonlinear flows
149 seen in figures 4(c) and 4(d) in the character of the nonlinear flows. Strands in nonlinear flows

150 experience a distribution of local strain rates which lead to a distribution of local mixing times
151 $g(\tau)$. We generate the distribution of Lagrangian strain rates as follows: We track the length r
152 of 10^4 line elements (with initial length $r_0 \equiv 1$) in these nonlinear flows by solving $\frac{d\vec{r}}{dt} = \vec{r} \cdot \vec{\nabla} \vec{u}$
153 along the trajectory of the center of the line elements. The Lagrangian strain rate is extracted for
154 each line element using its relation to growth of line element in an extensional flow,
155 $\dot{\gamma}(t) = \frac{1}{t} \log\left(\frac{r}{r_0}\right)$ for chaotic flows, and in a simple shear flow, $\dot{\gamma}(t) = \frac{1}{t} \left[\sqrt{\left(\frac{r}{r_0}\right)^2} - 1 \right]$ for non-
156 chaotic flows. The distribution of strain rates at any time is extracted from the ensemble of
157 Lagrangian strain rates at that time. Finally, using Eq. (4) (τ_{ext} for chaotic and τ_{ss} for non-
158 chaotic flow), we calculate the distribution of mixing times $g(\tau)$. Figure 5(a) presents $g(\tau)$ for
159 the chaotic and non-chaotic cases. We note that the width of $g(\tau)$ grows exponentially with
160 decreasing diffusivity in the chaotic flow whereas $g(\tau)$ reaches an asymptotic form in the non-
161 chaotic flow.

162 To account for the impact of the distribution of strain rates on the decay of reversibility, we
163 propose a modified Ranz model wherein we compute the weighted average return fraction

164 $R_{fMR}(\tau_{<\dot{\gamma}>}) = \int_0^{\infty} R_f(\tau) g(\tau) d\tau$. Figures 5(b) and 5(c) indicate that the modified Ranz model

165 captures the observed decay of $R_f(\tau_{<\dot{\gamma}>})$ for both flows over an extensive range of diffusivities.

166 Thus, the modified Ranz model provides a unified treatment of both chaotic and non-chaotic
167 flows. We note that return fraction in a chaotic flow with islands would decay faster initially due
168 to exponential stretching of the chaotic regions as predicted above, followed by slower diffusive
169 decay due to the islands [19].

170 C. Distinction in the zero diffusivity limit

171 To understand if there is a fundamental distinction between chaotic and non chaotic flows in the
172 context of SCDI, we explore the evolution of return fraction in chaotic and non-chaotic flows
173 using the modified Ranz model in the limit $D \rightarrow 0$. Exploration of this limit is motivated by the
174 observation that, while R_{fMR} in non-chaotic flows has already reached an asymptotic curve
175 (distinct from the master return curve of linear flows) for $D = 5.7 \times 10^{-10}$ [Fig. 5(c)], the
176 dependence of R_{fMR} on $\tau_{\langle j \rangle}$ in chaotic flows becomes increasingly weak [Fig. 5(b)]. Based on
177 our modified Ranz model, we can identify the origin of this distinction of the nonlinear chaotic
178 flow in the persistent growth of the tails of $g(\tau)$; this growth arises from the strong exponential
179 dependence of the local mixing time τ_{ext} on the strain of the fluid element. As a result of these
180 tails, R_{fMR} of the global flow is the combined effect of many fluid elements that are fully mixed,
181 many that are unmixed for any finite D , and a small fraction (vanishingly small in the limit
182 $D \rightarrow 0$) with an intermediate state of mixing that is sensitive to the precise value of D . When
183 this weak dependence R_{fMR} on $\tau_{\langle j \rangle}$ for chaotic flows is expressed in terms of differential
184 reversibility [lines labeled A,B,C,D,E in Fig. 5(d)], the trend indicates that the efficiency of
185 reversal becomes completely insensitive to differences in diffusivity (i.e, $\phi \rightarrow 1$ as $D \rightarrow 0$). In
186 comparison, the asymptotic form of the R_{fMR} curve for non-chaotic flows results in an
187 asymptotic form of differential reversibility [red line labeled NC in Fig. 5(d); different from the
188 master differential reversibility curve (black line labeled Master)] at finite values of diffusivity.
189 Thus, in the limit of infinitesimal diffusion, the underlying chaotic dynamics leads to complete
190 insensitivity to different levels of diffusion, in distinct contrast to the non-chaotic case.

191

192 **V. CONCLUSION**

193 We have shown that, beneath the dramatically different rates of decay of reversibility observed
194 in chaotic and non-chaotic flows, there exists significant unity in the evolution: i) all linear
195 flows lead to a universal decay of reversibility (R_f) when viewed in an appropriately scaled time
196 domain, and ii) a simple analysis that accounts for the distribution of strain rates successfully
197 captures the decay in both chaotic and non-chaotic, nonlinear flows. Interestingly though, in the
198 limit of infinitesimal diffusion, our analysis predicts a qualitative distinction between chaotic and
199 non-chaotic, nonlinear flows with respect to differential reversibility. We emphasize that the
200 distinction in this asymptotic behavior arises due to the interplay of dynamics, the distribution of
201 rates, and diffusion, and not due to chaos acting as an intrinsic source of irreversibility. Finally,
202 we note that our study indicates that a baker's transformation (with a single rate of strain) would
203 be the optimal flow with which to implement Heller's separation strategy with respect to both
204 rate and efficiency.

205 **Acknowledgements**

206 We thank Dr. Scott Verbridge and Dr. Emmanuel Villermaux for valuable suggestions. We
207 acknowledge support from the National Science Foundation (CTS-0529042) and the Department
208 of Energy (DE-FG02-05ER46250).

209 **REFERENCES**

210 [1] B. Misra, I. Prigogine, and M. Courbage, Proc. Nat. Acad. Sci. USA **76**, 3607 (1979).

211 [2] J. L. Lebowitz, Phys. Today **46**, 32 (1993).

212 [3] G. Drazer, J. Koplik, B. Khusid, and A. Acrivos, J. Fluid Mech. **460**, 307 (2002).

213 [4] D. J. Pine, J. P. Gollub, J. F. Brady, and A. M. Leshansky, Nature **438**, 997 (2005).

214 [5] P. Gaspard, *Chaos, scattering and statistical mechanics* (Cambridge Univ. Press, New
215 York, 1998), p.250-253.

216 [6] D. Levesque, and L. Verlet, J. Stat. Phys. **72**, 519 (1993).

217 [7] L. Corte, P. M. Chaikin, J. P. Gollub, and D. J. Pine, Nat. Phys. **4**, 420 (2008).

218 [8] W. E. Ranz, Aiche J. **25**, 41 (1979).

219 [9] J. P. Heller, Am. J. Phys. **28**, 348 (1960).

220 [10] G. I. Taylor, *Illustrated Experiments in Fluid Mechanics* (MIT Press, Cambridge, 1972),
221 p.47-54.

222 [11] H. Aref, and S. W. Jones, Phys. Fluids A: Fluid Dynamics **1**, 470 (1989).

223 [12] J. M. Ottino, *The kinematics of mixing : stretching, chaos, and transport* (Cambridge
224 Univ. Press, Cambridge, 1997), p.213-214.

225 [13] P. Dutta, and R. Chevray, Experimental Thermal and Fluid Science **11**, 1 (1995).

226 [14] G. L. Leal, *Laminar Flow and Convective Transport Processes: Scaling principles and*
227 *asymptotic analysis* (Butterworth-Heinemann Stoneham, 1992), p.77,171-172.

228 [15] T. Tél, M. Gruiz, and K. Kulacsy, *Chaotic dynamics: an introduction based on classical*
229 *mechanics* (Cambridge University Press, Cambridge, 2006), p.262-263.

230 [16] M. M. Alvarez, F. J. Muzzio, S. Cerbelli, A. Adrover, and M. Giona, Phys. Rev. Lett. **81**,
231 3395 (1998).

232 [17] G. I. Taylor, and A. E. Green, Proc. R. Soc. Lond. A-Math. Phys. Sci. **158**, 0499 (1937).

233 [18] J. D. Kirtland, G. J. McGraw, and A. D. Stroock, Phys. Fluids **18**, 13 (2006).

234 [19] P. B. Rhines, and W. R. Young, J. Fluid Mech. **133**, 133 (1983).

235

236

237

238 Figures and Captions:

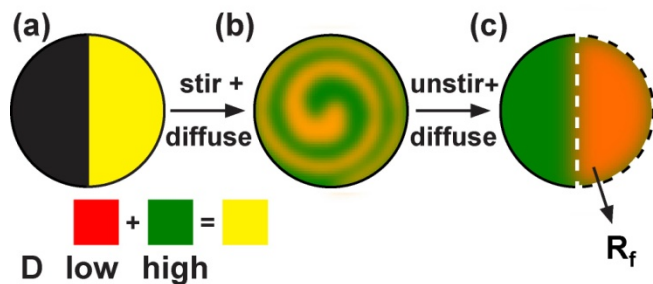
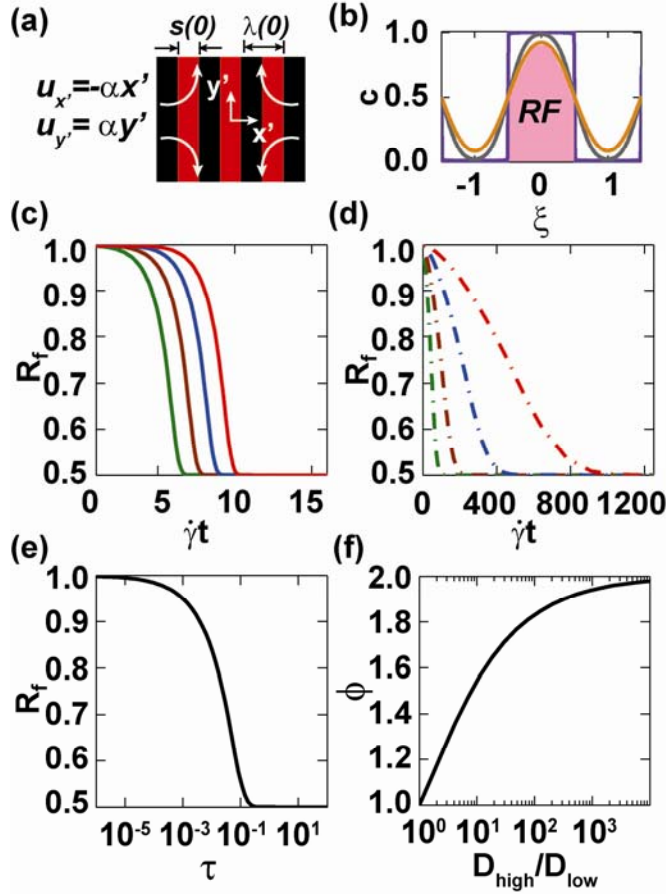
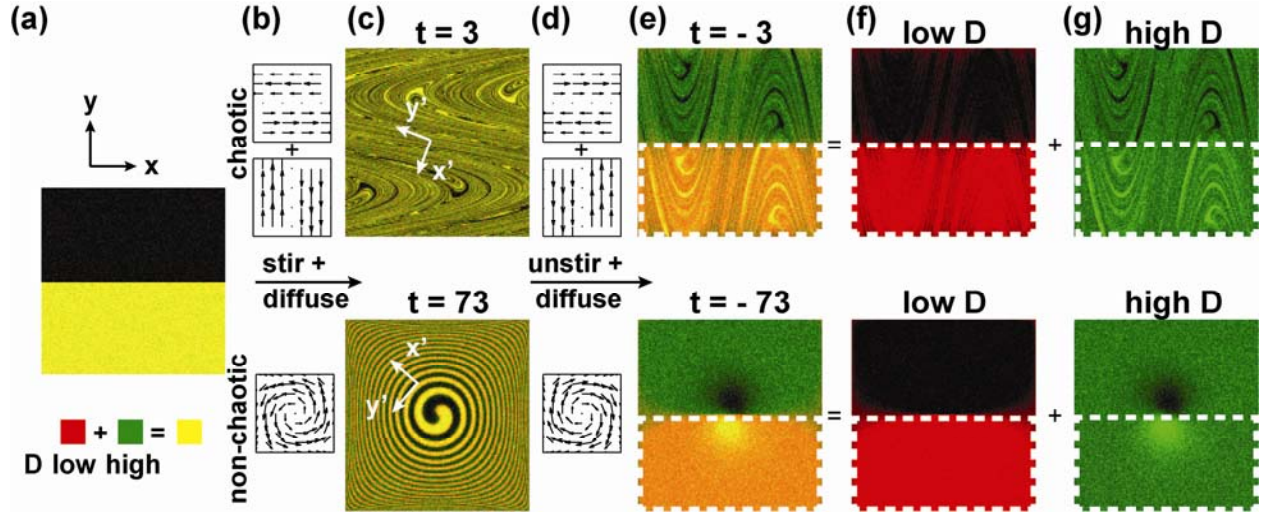


FIG. 1. (Color Online) Schematic representation of Separation by Convective Diffusive Irreversibility (SCDI). Concentration profiles of a one-to-one mixture (yellow) of two solutes of different diffusivities (green = high diffusivity, red = low diffusivity) (a-c) State of mixture (a) initially segregated from miscible carrier fluid (black) before stirring, (b) after stirring in a Stokes flow and (c) after reversing the flow (“unstirring”). The white dashed line in (c) represents the original volume occupied by the mixture in which return fraction R_f is evaluated. High diffusivity solute is distributed uniformly over the domain in (c).



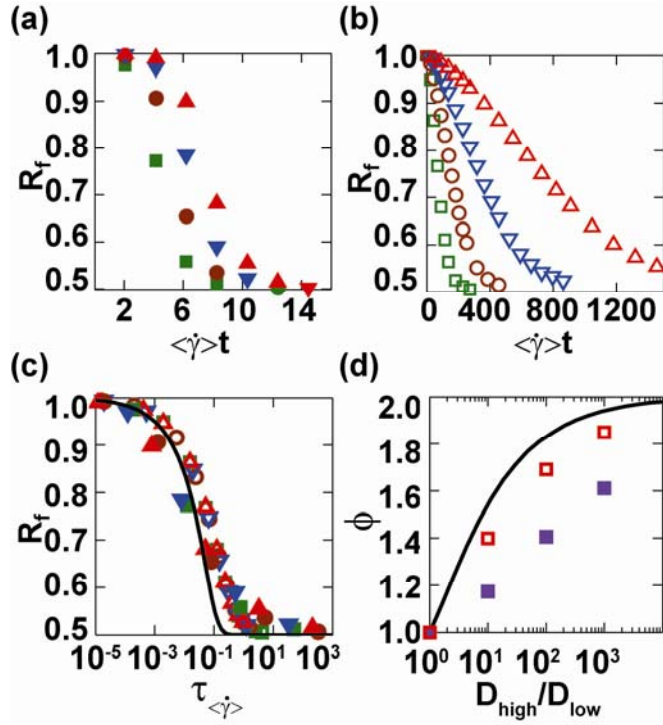
249

250 **FIG. 2. (Color Online)** SCDI in linear flows. **(a)** Initial concentration distribution of a diffusive
 251 solute (red) in the frame of reference of the strand (x', y') . **(b)** Concentration profile $c(\xi, \tau)$
 252 predicted by the Ranz model [Eq. (5)] initially ($\tau = 0$; violet curve), after stirring, ($\tau_{stir} = 0.02$;
 253 gray curve), and after unstirring ($\tau_{unstir} = 0.04$; orange curve). Return fraction R_f is defined as
 254 the area of shaded region. **(c-d)** Decay of R_f for (c) extension (solid lines) and (d) simple shear
 255 (dash-dot lines) as a function of total strain, $\dot{\gamma}t$, for four different diffusivities [from left to right,
 256 5.7×10^{-7} (green), 5.7×10^{-8} (brown), 5.7×10^{-9} (blue), 5.7×10^{-10} (red)]. **(e)** The master return curve
 257 $R_f(\tau_{stir})$ for all linear flows and pure diffusion. **(f)** The master curve of maximum differential
 258 reversibility, ϕ [Eq. (1)] for all linear flows plotted as a function of the ratio of diffusivities.



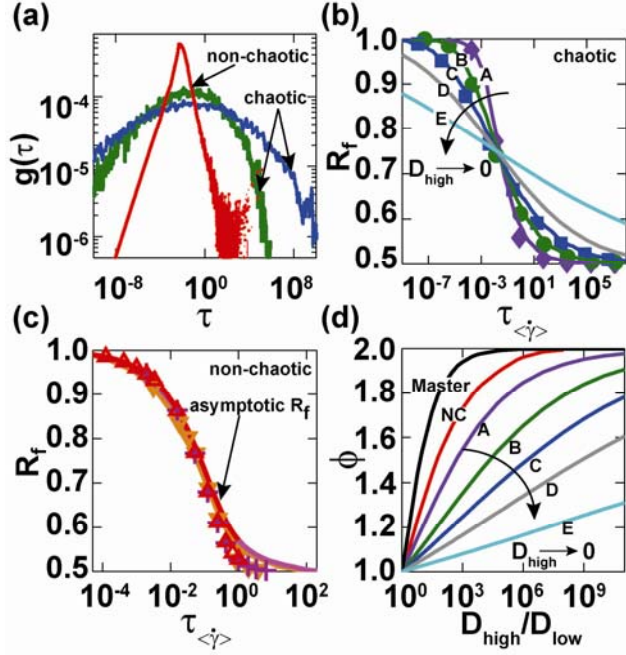
259

260 **FIG. 3. (Color Online)** SCDI in nonlinear Stokes flows. Evolution of concentration profiles of a
 261 one-to-one mixture of two tracers of different diffusivities $D_{high} = 5.7 \times 10^{-7}$ (green) and
 262 $D_{low} = 5.7 \times 10^{-10}$ (red), (diffusion is non-dimensionalized by $[H^2/T_{cyc}]$, where H is the height of
 263 the flow domain, T_{cyc} is the time period of the chaotic flow) in the chaotic (first row) and the
 264 non-chaotic (second row) flows. **(a)** Initial concentration profile with mixture in the lower half of
 265 the domain. **(b)** Schematic representation of the velocity fields used for stirring. **(c)**
 266 Concentration profile after stirring for t cycles ($t = 3$ for chaotic, $t = 73$ for non-chaotic)
 267 equivalent to the same mixing time τ of 0.24 and 0.00024 for the two diffusivities in both flows.
 268 **(d)** Velocity fields used for un-stirring. **(e)** Concentration profiles after un-stirring for the t
 269 cycles. The white dashed line indicates the region where the solutes were present initially in (a).
 270 **(f-g)** Individual concentration profiles after unstirring of (f) low diffusivity solute and (g) the
 271 high diffusivity solute. These distributions in (f) and (g) add up to give (e).



272

273 **FIG. 4. (Color Online)** Characteristics of SCDI in nonlinear Stokes flows. **(a-b)** R_f as a function
 274 of total strain (the mean strain rate $\langle \dot{\gamma} \rangle$ is 2.07 for the chaotic flow and 2.275 for the non-
 275 chaotic flow) for (a) the chaotic flow [$D=5.7 \times 10^{-7}$ (■), 5.7×10^{-8} (●), 5.7×10^{-9} (▼), 5.7×10^{-10} (▲)]
 276 and (b) the non-chaotic flow [$D=5.7 \times 10^{-7}$ (□), 5.7×10^{-8} (○), 5.7×10^{-9} (▽), 5.7×10^{-10} (△)]. **(c)** R_f as a function of mixing time $\tau_{\langle \dot{\gamma} \rangle}$ [with mean strain rates as in (b) and adjusted
 277 strand widths $s_0 = 0.375 H$ for the chaotic ($r^2 > 0.99$) and $1.25 H$ for the non-chaotic flow ($r^2 > 0.99$)]. **(d)** Maximum differential reversibility ϕ as a function of the ratio of diffusivities
 278 for pure diffusive case [black line, same as Fig. 2(e)], chaotic flow (■), and non-chaotic flow
 279 (□).
 280
 281



282

283 **FIG. 5. (Color Online)** SCDI in the limit of infinitesimal diffusion using the modified Ranz
 284 model. **(a)** Mixing time distribution $g(\tau)$ in the chaotic flow for two diffusive solutes ($D = 5.7 \times$
 285 10^{-16} (\bullet), $D = 5.7 \times 10^{-31}$ (\blacklozenge)) and in the non-chaotic flow for a diffusive solute ($D = 5.7 \times 10^{-16}$
 286 (\bullet)), for $\tau_{<j>} = 0.024$. **(b-c)** Return fraction R_f obtained from numerical simulation as a function
 287 of mixing time $\tau_{<j>}$ for (b) the chaotic flow (diffusivities 5.7×10^{-7} (\blacklozenge), 5.7×10^{-16} (\bullet) and 5.7
 288 $\times 10^{-31}$ (\blacksquare)) and (c) the non-chaotic flow (5.7×10^{-4} (\blacktriangledown), 5.7×10^{-7} (\blackplus), 5.7×10^{-10} (\blacktriangle)).
 289 Comparison with the return fraction based on modified Ranz model $R_{fMR}(\tau_{<j>})$ is shown using
 290 solid lines of the corresponding color for each diffusivity and flow [s_0 values in Fig. 3(c)]. In
 291 addition, in (b), return fraction $R_{fMR}(\tau_{<j>})$ corresponding to diffusivities $D = 5.7 \times 10^{-65}$ ($-$;D)
 292 and $D=5.7 \times 10^{-257}$ ($-$;E) are plotted indicating the trend in R_f as $D \rightarrow 0$. **(d)** Maximum
 293 differential reversibility ϕ as a function of ratio of the diffusivities. The master ϕ curve for pure
 294 diffusion ($-$; Master), the asymptotic ϕ curve for non-chaotic flow as predicted by the modified

295 Ranz model (-; NC), and trends for the chaotic case for D_{high} of 5.7×10^{-7} (-;A), 5.7×10^{-16} (-;B),
296 5.7×10^{-31} (-;C), 5.7×10^{-65} (-;D) and 5.7×10^{-257} (-;E) as predicted by the modified Ranz model.